Matrix-Isolation Infrared and Theoretical Studies of the Glycine Conformers

S. G. Stepanian,[†,‡] I. D. Reva,[‡] E. D. Radchenko,[‡] M. T. S. Rosado,[§] M. L. T. S. Duarte,[§] R. Fausto,[||] and L. Adamowicz*[,†]

Department of Chemistry, University of Arizona, Tucson, Arizona 85721, Institute for Low Temperature Physics and Engineermg, National Academy of Sciences of Ukraine, 47 Lenin Avenue, Kharkov 310164 Ukraine, Department of Chemistry, Faculty of Science, lJniversity of Lisbon, R. Ernesto de Vasconcelos, ed. C1 1700 Lisboa, Portugal, and Department of Chemistry, University of Coimbra, P-3049 Coimbra, Portugal

Received: October 21, 1997

The IR spectra of nonionized glycine and its deuterated derivatives isolated in the low-temperature argon matrices have been measured, and for the first time the infrared spectral characteristics of the three most stable conformers have been determined and assigned. Correlated level *ab initio* and density functional theory (DFT) calculations of IR frequencies and intensities with extended basis sets were performed and their results were employed to separate the bands of the glycine conformers in the experimental spectra and to assist the assignment. The intramolecular interconversion, conformer **III** ⇒ conformer **I**, which is observed in the matrices at temperatures higher than 13 K, was found to cause a significant decrease of the band intensities of conformer **III** in the spectra. This phenomenon was used to distinguish the vibrational bands of this conformer from the bands of the other conformers. The reliability of the Møller−Plesset second-order perturbation theory (MP2) method and the DFT method with the three-parameter density functional, Becke3LYP, in the prediction of the IR spectra of the nonionized glycine conformers was examined. We found that the DFT/Becke3LYP method with aug-cc-pVDZ basis set yields vibrational frequencies of the glycine conformers very similar to the MP2 results. Both DFT and MP2 results are in the excellent agreement with the experimental data.

1. Introduction

The simplest aminoacid, glycine, is one of the most important biological compounds. In the solid state and in solutions glycine is known to exist in the zwitterion form,[1] $NH_3^+-CH_2-COO^-$, but in the gas-phase glycine exists in nonionized form,[2] NH_2-CH_2-COOH. The internal rotation about the C−C, C−N, and C−O bonds results in several glycine conformers. The determination of the spectral and structural characteristics of the conformers of glycine, as well as other natural aminoacids, is of great interest because of their relation to the aminoacid units in peptides. Moreover, the assignment of the gas-phase glycine spectrum is of importance to radioastronomy in identification of interstellar aminoacids.[3]

The investigation of the gaseous glycine is difficult due to its thermal instability. Similar to other aminoacids, glycine decomposes before melting. Only a few experimental investigations of the gaseous glycine have been carried out during the past two decades. The first microwave spectroscopic results were presented by Brown et al.[4] and Suenram et al.[5] These studies identified conformer **II** (Figure 1) as the only gas-phase form of glycine and disagreed with the results of the earlier ab initio calculations which concluded that conformer **I** should be the lowest energy form.[6] The microwave spectrum of this conformer was observed a few years later by Suenram et al.[7] Accurate values of the rotational constants and dipole moments of the two low-energy glycine conformers, **I** and **II**, were determined in the more recent microwave studies.[8,9] The difficulty in the observation of conformer **I** in the microwave spectra was caused by its significantly lower dipole moment than the dipole moment of conformer **II**. Since the other low-energy conformers of glycine also have low dipole moments, their identification in microwave spectra is difficult. Thus, the theoretically predicted conformer **III** is hardly registered by the microwave spectroscopy.

The molecular structure of the gaseous glycine were determined by Iijima et al.[2] in an electron-diffraction study. Again conformer **I** was proven to be the most stable form in the gas phase, but at a temperature of 219 °C, about 24% of the compound was detected to appear as a mixture of minor conformers which were supposed to be conformers **II** and **III**.[2] However, these conformers are different from each other only in the position of the hydrogens and they are indistinguishable by their electron scattering intensities.[2] Thus, the question of the conformational structure of glycine in the gas phase has remained open.

The conformational behavior of glycine has been the subject of very extensive theoretical studies.[10−20] All calculations have been consistent in predicting that the conformer **I** is the most stable form. However the stability order and the structures of the other glycine conformers depended on the level of theory and the basis set used in the calculations. The comparison of the relative energies of the glycine conformers calculated at the HF and MP2 levels shows that the former method overestimates the energy gap between conformer **I** and the other conformers.[12,17] The DFT calculations of the structure and relative stabilities of the glycine conformers[11,14] produced results which are very similar to the results of the MP2 method. The

* Corresponding author.
[†] University of Arizona.
[‡] National Academy of Sciences.
[§] University of Lisbon.
[||] University of Coimbra.

S1089-5639(97)03397-5 CCC: $15.00
Published on Web 01/22/1998

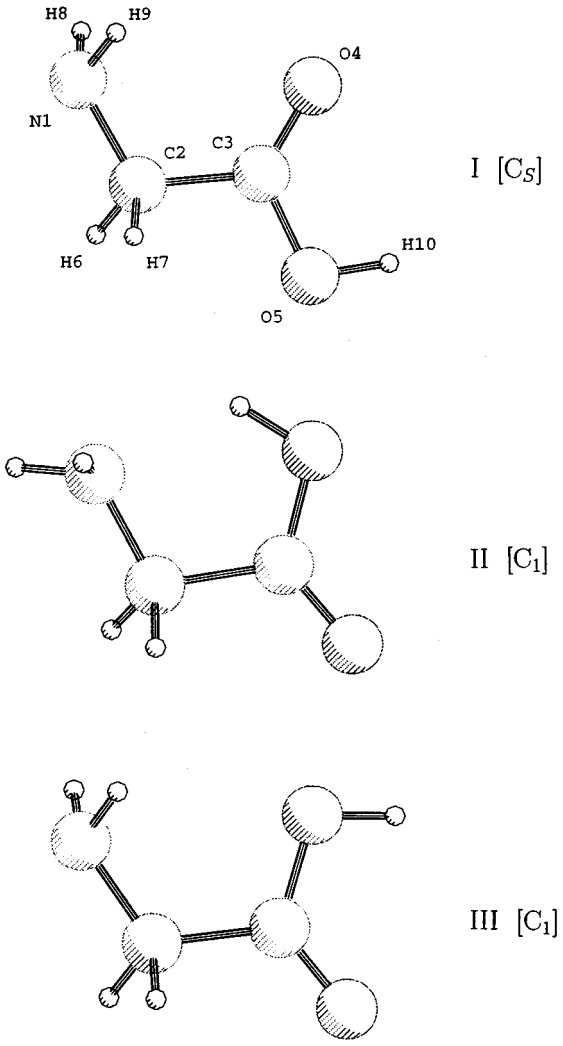

Figure 1. The lowest energy glycine conformers **I**, **II**, and **III**.

sophisticated investigations of the potential energy surface of glycine[12,15,16,19] allowed identification of as many as eight minimum-energy conformers and the estimation of the barriers of the conformer interconversions. Some of these barriers were predicted to be quiet small.[15,19]

The results of quantum-chemical calculations of the relative stabilities of the glycine conformers have shown that, besides the early observed conformers **I** and **II**, at least one more conformer, namely conformer **III** (Figure 1), may exist in the gas phase. As it is seen in the molecular structures of the low-energy conformers in Figure 1, they differ in the intramolecular H-bonds: bifurcated $NH_2\cdots O{=}C$ H-bond in conformer **I**, $N\cdots H{-}O$ H-bond in conformer **II** and bifurcated $NH_2\cdots O{-}C$ H-bond in conformer **III**. IR spectroscopy could be a very suitable tool to investigate the glycine conformational structure, since the IR spectra are very sensitive to the intramolecular H-bonding. However, the low thermal stability of glycine precludes IR study in the gas phase because it is not possible to obtain a concentration of the glycine in the gas phase which is sufficient to register its IR spectra. In such situations a combined use of the IR spectroscopy and matrix isolation technique can be very helpful[21] since it allows separation of the matrix deposition process, which may be very long, from the registration of the IR spectrum of the sample. Also, the inert-gas matrix environment hinders the rotation of the molecules studied and excludes the presence of rotational structures in the IR bands, simplifying the interpretation of the matrix IR spectra in comparison with gaseous ones.

Our first attempts to freeze a complete set of the glycine low-energy conformers in the Ar matrices were unsuccessful. In these experiments the samples were deposited at 16−17 K. From our previous experiments we found that this temperature range is optimal to prepare samples with minimal scattering. We supposed that the low energy barriers between the glycine conformers predicted theoretically[19] might lead to easy interconversion of the conformers in the low-temperature matrices. To elucidate this question further, we performed a search for optimal experimental conditions which allow us to deposit a complete set of the low-energy glycine conformers in the matrices.[22] In the course of this study, IR spectra were measured for samples deposited at temperatures ranging from 19 to 5.5 K. We found that, for samples deposited at temperatures below 13 K, additional bands appear in the IR spectra of matrix-isolated glycine. These bands may correspond to a new glycine conformer which did not appear at higher temperatures because it immediately interconverted to lower energy rotamers. Various matrix gases (Ne, Ar, and Kr) were used to prove that the observed phenomenon is indeed due to the presence of an additional glycine conformer and not to matrix splittings. In this study[22] we also explained why the matrix IR spectra of glycine obtained by Grenie et al.[23] because the samples deposited at 20 K did not contain the conformational splittings which appeared at lower temperatures.

In continuation of these studies, in this work we undertook a detailed investigation of the conformational composition of the gaseous glycine isolated in low-temperature matrices. In this paper we present results of simultaneous observation of the three low-energy glycine conformers. The IR spectral characteristics of these conformers (conformers **I**, **II**, and **III)** are assigned on the basis of the comparison with the data calculated using the DFT and MP2 methods. The reliability of these methods in predicting vibrational frequencies and intensities of nonionized aminoacids is discussed.

2. Experimental Details

The thermal instability of glycine creates certain problems with the sample preparation. The Knudsen cell was used in the present work to evaporate glycine. It was necessary to first determine the optimal evaporation temperature, which is high enough to yield samples with sufficient concentration of the compound but still sufficiently low to prevent decomposition of the compound. A low-temperature quartz microbalance was used to measure the intensity of the gaseous flow of glycine. In our design of the deposition system, the minimal temperature at which the flow of glycine was found sufficient for the sample preparation was ≈ 160 °C. The quartz microbalance was used to measure the gaseous flow of the substance studied and of the matrix gas. It allowed us to control the concentration of the glycine in the matrix and to avoid the appearance of autoassociates.

The measurements were carried out for glycine (glycine-d_0) and for its deuterated derivatives: *C,C*-d_2-glycine, *N,N,O*-d_3-glycine, and the fully deuterated glycine which will be denoted as glycine-d_2, glycine-d_3, and glycine-d_5, respectively. The matrix samples were prepared by simultaneous deposition of the substance and the matrix gas onto a cooled CsI substrate. The matrix gas was 99.99% Ar. The substrate temperature was 12−13 K during matrix preparation, and that allowed us to prevent interconversion of the glycine conformers in the matrices. Commercially available glycine and its isotopomers

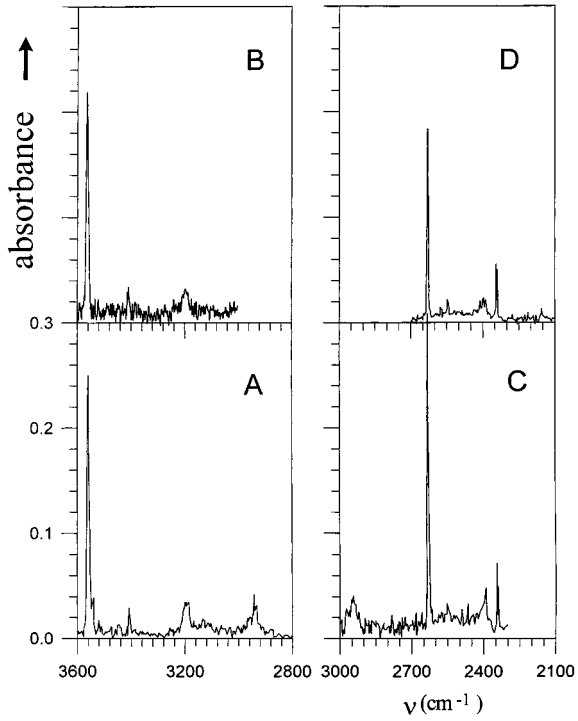

Figure 2. The high-frequency regions of the matrix IR spectra of the glycine isotopomers: glycine-d_0 (A), glycine-d_2 (B), glycine-d_3 (C), glycine-d_5 (D). The spectra were recorded for the samples deposited at 13 K. Matrix ratio is 1:1000 for glycine-d_0 and 1:750 for other isotopomers.

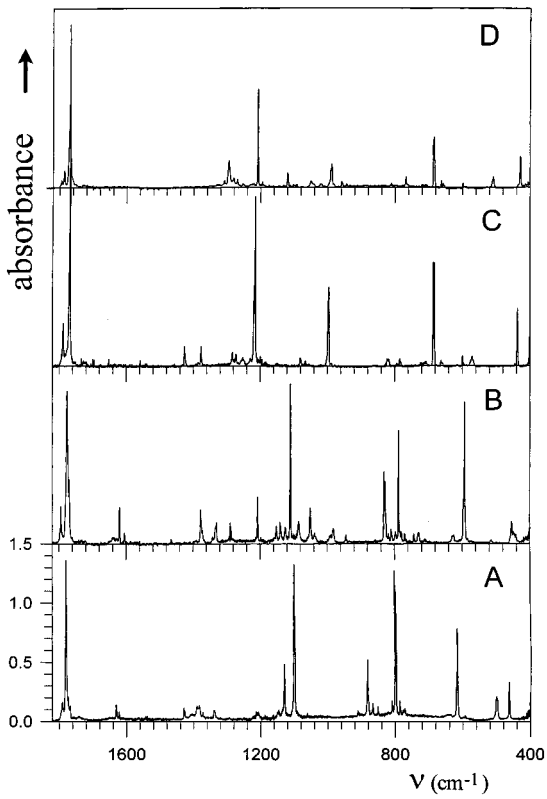

Figure 3. The fingerprint regions of the matrix IR spectra of the glycine isotopomers: glycine-d_0 (A), glycine-d_2 (B), glycine-d_3 (C), glycine-d_5 (D). The spectra were recorded for the samples deposited at 13 K. Matrix ratio is 1:1000 for glycine-d_0 and 1:750 for other isotopomers.

were used in the experiments. They were evaporated from the Knudsen cell at 170 °C for glycine, 161 °C for glycine-d_2, 176 °C for glycine-d_3, and 169 °C for glycine-d_5. The thermostatting accuracy was 0.2 °C. Ar flow stability was achieved with a stable gas pressure over the solid argon at 77 K and was adjusted by a needle valve. The fill-up helium cryostat used in our matrix-isolation IR experiments was described elsewhere.[24] The IR spectra were registered with the updated SPECORD IR 75 spectrometer in the range 4000−400 cm^{-1} with the resolution of 3 cm^{-1} in the range 4000−2500 cm^{-1} and with the resolution of 1 cm^{-1} in the range 2500−400 cm^{-1}. The spectrometer was sealed and blown through with dry nitrogen during the experiment to exclude any influence of the atmospheric H_2O and CO_2 vapors. Firstly, the IR spectra were recorded for glycine-d_0, glycine-d_2, glycine-d_3, and glycine-d_5 immediately after sample deposition. These spectra are shown in Figures 2 and 3. They do not contain any bands of the glycine decomposition products. Only trace amounts of CO_2 are found in the samples (the characteristic doublet band of the CO stretching vibrations at 2344/2339 cm^{-1}) which is most probably due to CO_2 absorbed on the surface of the solid compounds used for the experiment. To separate the IR bands of conformer **III** from other conformers, additional experiments were carried out for all isotopomers. In these experiments, the samples deposited at 12−13 K were heated up to 20 K and after 30 min they were chilled and their spectra were recorded. At 20 K argon matrix remains rigid enough so that the translational diffusion of the guest molecules is negligible. Thus, neither dimer formation of the molecules studied nor the sufficient repacking of the matrix environment were possible. However, the temperature of 20 K was high enough for conformer **III** to interconvert to the lower energy conformer **I**. Comparing the spectra obtained before and after annealing, we were able to identify the bands due to conformer **III**.

3. Theoretical Methods

The main goal of the calculations in the present study was to simulate the IR spectral characteristics of the most stable glycine conformers, which were used to identify the conformers in the experimental matrix IR spectra. To achieve this goal we first searched for energy minima on the potential energy surface of glycine corresponding to the lowest energy conformers and then we calculated the IR frequencies and intensities for the minima using the harmonic approximation. Glycine, as the smallest aminoacid, is a suitable model to examine reliability of the theoretical methods used in the calculations of IR spectra. This kind of analysis will be helpful in our future matrix-isolation IR studies on other aminoacids and small peptides. Among the Hartree−Fock (HF), Møller−Plesset second-order perturbation theory (MP2) and DFT methods used to study the structure of the glycine conformers,[10−20] the two latter methods yield the results which are in best agreement with the results of microwave and electron diffraction studies.[2,4,5,7−9] The HF method failed to predict the correct relative energies and structure of the glycine conformers with the N···H−O intramolecular H-bond.[12,17] Therefore, in the present study we have used the MP2[25] and the DFT methods for the harmonic frequency calculations of the glycine conformers.

The DFT calculations were carried out with Becke's gradient exchange correction,[26] the Lee, Yang, Parr correlation functional,[27] and the Vosko, Wilk, Nusair correlation functional.[28] This three-parameter density functional, designated as B3LYP, was found to produce the most accurate glycine structural parameters compared with the microwave results.[11,14]

For geometry optimization and harmonic frequency calculations, we used three Dunning's correlation-consistent double-ζ basis sets.[29,31] The smallest basis set used in this study was

TABLE 1: Optimized Geometry Parameters (Angstroms and Degrees) of the Glycine Conformers Obtained in the DFT/B3LYP/aug-cc-pVDZ and MP2/aug-cc-pVDZ Calculations

		I		**II**		**III**	
	exptl[a]	DFT	MP2	DFT	MP2	DFT	MP2
C−N	1.467	1.450	1.456	1.471	1.474	1.452	1.458
C−C	1.526	1.524	1.523	1.535	1.535	1.527	1.526
C═O	1.205	1.211	1.220	1.208	1.218	1.211	1.220
C−O	1.355	1.359	1.367	1.344	1.352	1.359	1.368
C−H_6	1.081	1.100	1.102	1.099	1.101	1.100	1.101
C−H_7	1.081	1.100	1.102	1.098	1.101	1.100	1.102
N−H_8	1.001	1.018	1.021	1.014	1.017	1.017	1.020
N−H_9	1.001	1.018	1.021	1.015	1.018	1.017	1.020
O−H	0.966	0.971	0.974	0.986	0.988	0.972	0.975
N−C−C	112.1	115.9	115.4	111.5	111.0	119.3	118.8
C−C═O	125.1	125.8	125.8	122.8	122.9	124.0	124.2
C−C−O	111.6	111.4	111.0	114.0	113.9	113.5	112.9
C−C−H_6		107.5	107.5	107.5	107.6	106.0	106.1
C−C−H_7		107.5	107.5	106.6	106.4	105.9	106.1
H−C−H	107.0	105.7	106.1	106.9	107.3	105.6	106.0
C−N−H_8	113.3	110.4	109.4	112.6	111.8	111.2	110.1
C−N−H_9	113.3	110.4	109.4	112.3	111.4	111.2	110.1
H−N−H	110.3	105.8	105.0	107.7	107.2	106.6	105.7
C−O−H	112.3	107.2	106.1	105.1	104.0	106.5	105.3
N−C−C═O		0.0	0.0	173.2	171.2	179.3	179.3
N−C−C−O		180.0	180.0	−7.5	−9.9	−0.8	−0.8
O═C−C−H_6		123.4	123.4	48.1	45.7	55.1	55.5
O═C−C−H_7		236.6	236.6	−66.2	−69.1	−56.7	−56.9
C−C−N−H_8		58.3>	57.3	133.6	138.8	59.2	58.0
C−C−N−H_9		-58.3	-57.3	255.4	258.8	−59.4	−58.2
C−C−O−H		180.0	180.0	1.3	1.8	180.1	180.1

[a] From ref 2. In ref 2 some parameters were taken from HF/4-21G calculations.[7b] They are shown in italics.

the standard cc-pVDZ basis set. The two other sets were obtained from the first one by adding diffuse functions. The second basis set, denoted here as cc-pVDZ++, included only an s diffuse function on hydrogens and s and p diffuse functions on heavy atoms (the exponents of the diffuse functions were the same as in the standard aug-cc-pVDZ basis). The third basis set was the standard aug-ccpVDZ basis, which includes s and p diffuse functions on hydrogens and s, p, and d diffuse functions on heavy atoms. The previous theoretical studies of the potential energy surface of glycine identified eight minimum-energy geometries.[12,15,16,19] In this study we carried out frequency calculations for only the most stable conformers **I**, **II**, and **III** (Figure 1), which are supposed to exist in the gas phase. All calculations in this work were performed on IBM RS6000 workstations using the Gaussian94[32] quantum-mechanical program.

4. Results and Discussion

4.1. Structure and Relative Stabilities of the Glycine Conformers. The geometries of the three glycine conformers—**I**, **II**, and **III**—were fully optimized at the DFT/B3LYP and MP2 levels with the cc-pVDZ, cc-pVDZ++, and aug-cc-pVDZ basis sets (i.e., six sets of structural parameters were calculated for each conformer). In this section the structural parameters and rotational constants of the glycine conformers calculated at the DFT/B3LYP and MP2 levels of theory with the different basis sets are compared with the available experimental data to determine which method yields the most accurate results. For this comparison we use the experimental geometry parameters of the conformer **I**[2], as well as the rotational constants of the conformers **I** and **II** of the glycine-d_0 and glycine-d_2, and the rotational constants of the conformer **II** of the glycine-d_3.[8,9] The experimental and calculated geometries of conformers **I**, **II**, and **III** are presented in Table 1. Among the experimental parameters, those shown in italics in Table 1 were not derived from the experimental data but were assumed on the basis of previous ab initio calculations at the HF/4-21G level.[7b] The experimental and calculated rotational constants are summarized in Table 2.

The inclusion of the diffuse functions in the basis set leads to a significant improvement of the calculated structure of the main glycine conformer with respect to the experimental geometrical parameters at both the DFT/B3LYP and MP2 levels. The comparison of the DFT/B3LYP/aug-cc-pVDZ and MP2/aug-cc-pVDZ geometries with the experimental data (Table 1) shows that the DFT method is able to produce geometries with similar accuracy as the MP2 method. The mean differences between the calculated at the DFT/B3LYP level and observed geometry parameters are 0.010 Å and 1.6° for the bond lengths and the bond angles, respectively. The corresponding values for the MP2 method are 0.013 Å and 1.5°. The comparison of the calculated and the observed rotational constants (Table 2) also shows that the two methods give very similar results. The best agreement with experiment is obtained when the aug-cc-pVDZ basis set is applied in conjunction with the DFT/B3LYP method. In this case, the rotational constants are in even better agreement with the experiment than the MP2 results (Table 2).

When analyzing the calculated geometries of the three glycine conformers, we paid special attention to the conformation of the heavy atom backbone. The entry-level HF calculations with a small basis sets[19] predicted the planar backbone structure for all three conformers. Increasing the basis, by additional polarization functions and accounting for the electron correlation effects, led to nonplanar structures of the conformers **II** and **III**,[10,12,16,17] while conformer **I** still remains planar in all calculations. As it is seen from Table 1, at both the DFT/B3LYP and MP2 levels we obtain planar structures for conformer **I** and nonplanar structures for conformer **II**. In the latter case the torsion angle, NCC═O, is 173.23° and 171.23° at the B3LYP and MP2 levels, respectively. On the other hand,

TABLE 2: Rotational Constants (MHz) and Dipole Moments (Debye) of the Glycine Conformers Observed and Calculated with the aug-cc-pVDZ Basis Set

	I			II			III	
	exptl[a]	DFT	MP2	exptl[a]	DFT	MP2	DFT	MP2
				glycine-d_0				
A_c	10342	10283	10130	10130	10126	10021	9931	9849
B_c	3876	3832	3844	4071	4046	4042	3945	3952
C_c	2912	2883	2878	3007	2994	2988	2917	2915
μ	1.15b	1.17	1.30	5.45b	5.65	6.10	1.90	2.01
				glycine-d_2				
A_c	9318	9270	9138	9081	9068	8978		
B_c	3799	3756	3774	3989	3964	3959		
C_c	2832	2804	2799	2918	2904	2898		
				glycine-d_3				
A_c				9485	9480	9390		
B_c				3680	3655	3654		
C_c				2778	2764	2760		

[a] The rotational constants of the glycine-d_0, glycine-d_2, and glycine-d_3 are taken from ref 8. [b] From ref 9.

determination of whether conformer **III** has planar or nonplanar structure is not as clear. The potential energy surface of this conformer is extremely flat near the minimum. The deviation from the planarity determined in the calculations is less than 1°. The values of the torsion angle NCC═O calculated at the DFT/B3LYP and MP2 levels with the aug-cc-pVDZ basis set are 179.26° and 179.30°, respectively. It is notable that the energy difference between the nonplanar structures of the conformers **II** and **III** and their planar counterpairs is rather small. For example, the energy difference between the more stable non-planar form of the conformer **II** and its planar counterpart was predicted to be 0.21 kJ mol^{-1} at the B3LYP/DZP level,[11] 0.24 kJ mol^{-1} at the MP2/6-31++g** level,[16] 0.55 kJ mol^{-1} at the CISD/DZP level,[15] and 0.42 kJ mol^{-1} at the CCSD (T)/DZP level.[15] For conformer **III**, the calculation carried out at the CISD/DZP[15] and DFT/B3LYP/DZP levels[11] predicted the planar conformation to be the true minima, but at the same time the calculation at the MP2/6-311++G** level,[16] as well as our calculations at the MP2/aug-cc-pVDZ and B3LYP/aug-cc-pVDZ levels, predict that a nonplanar conformation is the true minimum. The flat potential energy surface near the equilibrium point predicted for the conformer **III** requires tighter thresholds in the geometry optimization. Therefore, for conformer **III**, we carried out an additional structure calculation using the keyword OPT═TIGHT, decreasing the convergence criteria 30 times. In this calculation we did not observe any significant changes in the energy; it decreased by less than 0.1 kJ mol^{-1}, and in the geometry, except for the value of the dihedral NCC═O angle, which increased by a few degrees. The DFT/B3LYP/aug-cc-pVDZ frequency calculations carried out for conformer **III** at the geometry obtained after the optimization with the conventional thresholds did not produce any imaginary frequencies. Nevertheless, the energy difference between the planar and nonplanar form of these conformers is lower than the energy of the zero-point twisting vibration, and from the experimental point of view, the planar structure is likely to be the most probable conformation.

The energies, zero-point energies (ZPEs), and the relative stabilities of the three most stable glycine conformers are summarized in Table 3. In the first place, the importance of the ZPE contribution in the prediction of the relative stabilities of the conformers, especially in the case of conformer **II**, should be noticed. As it is seen, the ZPE energies of conformer **II**, at both the DFT/B3LYP and MP2 levels, are higher than those of the conformers **I** and **III**. This leads to destabilization of the conformer **II** by 1.20 kJ mol^{-1} at the DFT/B3LYP/aug-cc-pVDZ level and by 1.72 kJ mol^{-1} at the MP2/aug-cc-pVDZ level. At the same time, the ZPE only slightly changes the relative energy of the conformer **III** with respect to the main conformer.

The DFT/B3LYP and MP2 methods yield very similar values of the relative energies of the glycine conformers. The relative energies of conformers **II** and **III** with respect to the main conformer are 3.60 and 6.84 kJ mol^{-1} at the DFT/B3LYP/aug-cc-pVDZ level and 3.96 and 7.14 kJ mol^{-1} at the MP2/aug-cc-pVDZ level. On the basis of analysis of the data presented in the Tables 1−3, we may conclude that the DFT/B3LYP method produces structures of the glycine conformers, which are in very good agreement with the experimental data and almost identical to the MP2 results. It allows us to hope that this method is also able to produce the vibrational frequencies and infrared intensities with high accuracy.

4.2. IR Spectral Characteristics of the Glycine Conformers. The electron diffraction[2] and microwave[4,5,7−9] studies demonstrated the presence of glycine conformers **I** and **II** in the gas phase. In our preliminary matrix isolation IR study,[22] we observed in the IR spectra some manifestations of an additional glycine conformer which, based on the results of the quantum-chemical calculations, is now supposed to be conformer **III**. If all three conformers are present in the samples, the experimental IR spectrum is a superposition of their spectra. To determine the spectral characteristics of the individual conformers, we have to separate their vibrational bands. This separation is based on the following data: (i) The results of the theoretical simulations of the IR spectra of the three glycine conformers.

(ii) The elimination of the bands of conformer **III** from the experimental spectrum. As was mentioned before, the low energy barrier of the conformer **III** ⇒ conformer **I** interconversion results in the disappearance of conformer **III** from the matrix at temperature above 13 K. This phenomenon was used to distinguish the bands of conformer **III** by comparing the IR spectra recorded before and after matrix annealing.

(iii) The experimental IR spectra measured for the glycine deuterated derivatives. The analysis of the isotopomer frequency shifts and their comparison with calculated shifts can provide additional support for the assignments.

The harmonic frequency calculations of the glycine conformers were carried out at the DFT/B3LYP level with the cc-pVDZ, cc-pVDZ++, and aug-cc-pVDZ basis sets, as well as at the MP2 level with the cc-pVDZ and cc-pVDZ++ basis sets. The disk space limitation precluded calculations at the MP2 level with the aug-cc-pVDZ basis set. The average divergences

TABLE 3: Energies (au), Relative Stabilities (ΔE)(kJ mol^{-1}), Zero-Point Vibrational Energies (ZPE[a]) (au), Total Energies Including the Zero-Point Vibrational Energies (au) and Relative Stabilities Including the Zero-Point Vibrational Energy (kJ mol^{-1}) of the Three Glycine Conformers. Values Taken from the Full Optimization and Frequency Calculations of the Conformers at the DFT/B3LYP and MP2 Levels of Theory

method		glycine **I**	glycine **II**	glycine **III**
DFT/cc-pVDZ	energy	−284.449 089 2	−284.448 205 8	284.446 602 4
	ΔE(DFT)	0.00	2.32	6.53
	ZPE	0.076 662 2	0.077 200 5	0.076 791 1
	total energy	−284.372 427 0	−284.371 005 3	−284.369 811 3
	ΔE(DFT + ZPE)	0.00	3.73	6.87
DFT/cc-pVDZ++	energy	−284.471 348 1	−284.470 071 7	−284.468 957 9
	ΔE(DFT)	0.00	3.35	6.27
	ZPE	0.076 423 8	0.076 887 4	0.076 489 2
	total energy	−284.394924 3	−284.393 184 3	−284.39 2460 7
	ΔE(DFT + ZPE)	0.00	4.57	6.45
DFT/aug-cc-pVDZ	energy	−284.482 215 4	−284.481 300 6	−284.479 601 0
	ΔE(DFT)	0.00	2.40	6.86
	ZPE	0.077 2785	0.077 736 7	0.077 268 6
	total energy	−284.404 936 9	−284.403 563 9	−284.402 332 4
	ΔE(DFT + ZPE)	0.00	3.60	6.84
MP2/cc-pVDZ	energy	−283.667 601 7	−283.666 091 8	−283.665 114 5
	ΔE(MP2)	0.00	3.96	6.53
	ZPE	0.076 831 1	0.077 375 4	0.076 917 6
	total energy	−283.590 770 6	−283.588 716 4	−283.588 196 9
	ΔE(MP2 + ZPE)	0.00	5.39	6.76
MP2/cc-pVDZ++	energy	−283.692 487 0	−283.691 202 9	−283.690 126 8
	ΔE(MP2)	0.00	3.37	6.20
	ZPE	0.077 045 8	0.077 699 2	0.077 225 1
	total energy	−283.615 441 2	−283.613 503 7	−283.612 901 7
	ΔE(MP2 + ZPE)	0.00	5.09	6.67
MP2/aug-cc-pVDZ	energy	−283.736 2692	−283.735 417 3	−283.733 727 0
	ΔE(MP2)	0.00	2.24	6.67
	ΔE(MP2 + ZPE[b])	0.00	3.96	7.14

[a] Zero-point vibrational energies were scaled applying the scaling factors SF1 and SF2 listed in Table 4. [b] ZPE from the MP2/cc-pVDZ++ calculation was used here.

TABLE 4: Mean Divergences (cm^{-1}) between the Calculated and Observed Frequencies of the Four Isotopomers of the Conformer I[a]

				glycine-d_0		glycine-d_2		glycine-d_3		glycine-d_5	
method	basis set	SF1	SF2	A	B	A	B	A	B	A	B
DFT	cc-pVDZ	0.96	0.97	49.5	16.5	35.5	17.8	32.1	22.9	31.3	15.6
				33.2	12.8	23.7	16.8	20.6	15.8	22.5	10.3
	cc-pVDZ++	0.95	0.98	40.8	14.9	28.6	16.2	27.7	19.5	26.7	16.9
				18.3	9.4	13.1	13.5	11.1	10.7	12.0	8.5
	aug-cc-pVDZ	0.96	0.99	44.1	11.8	30.2	9.5	29.9	8.7	27.5	9.9
				18.3	9.4	11.8	8.1	10.5	4.5	11.1	7.0
MP2	cc-pVDZ	0.95	0.95	75.5	19.4	57.0	20.2	55.7	22.9	51.8	16.1
				48.4	18.8	38.8	21.5	36.4	24.4	35.7	15.8
	cc-pVDZ++	0.95	0.97	61.7	11.9	44.8	15.0	46.5	13.9	41.9	11.6
				29.3	11.2	23.9	14.7	22.5	12.7	21.5	10.3

[a] The mean divergences calculated for the nonscaled and scaled frequencies are listed in the columns A and B, respectively. For each basis set and for the DFT/B3LYP and MP2 levels of theory, the mean divergences were calculated for all frequencies (presented in the first row) and for the frequencies below 2000 cm^{-1} (presented in the second row).

between the calculated and observed frequencies were calculated for the four isotopomers of the glycine **I** conformer to determine which theoretical method yields the most accurate isotopomer frequencies. The comparison is presented in Table 4. The data shown in column A of Table 4 were obtained with nonscaled calculated frequencies. For all the levels of theory used in this study, we determined the optimal scaling factors which allowed us to obtain the minimal mean divergencies between the calculated and observed frequencies. Two scaling factors, SF1 and SF2, were determined for the frequencies calculated with each basis set: SF1 for the X(C,N,O)-H stretching vibrations and SF2 for all other vibrations. The mean divergences calculated for the scaled theoretical frequencies are presented in column B in Table 4 along with the values of the scaling factors. Table 4 includes two rows for each basis set. In the first row the mean divergences were calculated for all observed frequencies. In the second row the mean divergences were calculated only for the frequencies below 2000 cm^{-1} (i.e., for all frequencies, excluding X(C,N,O)-H stretching vibrations).

The following conclusions may be derived from the analysis of the data presented in Table 4: (i) The best agreement between the calculated and observed frequencies is observed when the DFT/B3LYP method with the aug-cc-pVDZ basis set is employed. The mean divergence is only about 10 cm^{-1}. This value was obtained using scaled frequencies with the scaling factors SF1 = 0.96 and SF2 = 0.99 (Table 4).

(ii) The MP2 method also yields frequencies which are in good agreement with the experimental data after scaling. The mean divergence calculated for the MP2/cc-pVDZ++ frequencies is about 13 cm^{-1}, although the scaling factors employed here are smaller then the ones obtained for the DFT/B3LYP/aug-cc-pVDZ frequencies.

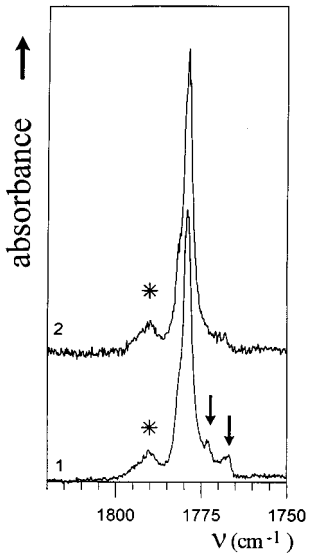

Figure 4. The region of the C═O stretching vibrations of glycine-d_0 conformers. (1) IR spectrum recorded after matrix deposition at 13 K. (2) IR spectrum recorded after matrix annealing at 20 K for 30 min. Asterisks (*) mark the bands assigned to conformer **II**. Down arrows (↓) mark the bands assigned to conformer **III**.

(iii) Augmentation of the basis set by additional diffuse functions significantly improves the agreement between the calculated and observed frequencies at both the DFT/B3LYP and MP2 levels of theory. As mentioned above, the inclusion of the diffuse functions is particularly important to predict correctly the relative energy and the structure of the conformer **II**. This is most probably due to the strong intramolecular N···H−O H-bonding interaction present in this conformer whose description requires diffuse orbitals in the basis set. For the same reason, the augmentation of the basis set with diffuse functions can be expected to produce better agreement between the calculated and observed IR frequencies.

(iv) In almost all the cases considered increasing the number of the deuterium atoms in the glycine molecule led to decrease of the mean frequency divergences (Table 4). This may be simply explained by the decrease of most frequency values upon deuteriation, which results in a decrease of the mean divergence.

The analysis of the mean divergences presented in Table 4 shows that the DFT/B3LYP/aug-cc-pVDZ method yields the most accurate vibrational frequencies of all the considered deuterated derivatives of the main glycine conformer **I**. These frequencies have been used to identify the bands of the minor conformers in the experimental spectra.

The observed and calculated (at the DFT/B3LYP/aug-cc-pVDZ level) IR frequencies and intensities of conformers **I**, **II**, and **III** are presented in Tables 5−8 for glycine-d_0, glycine-d_2, glycine-d_3 and glycine-d_5, respectively. In these tables the results of the potential energy distribution (PED) analysis are also given. If several of the calculated frequencies belonging to the different conformers are assigned to a single observed band, the PEDs presented in the tables correspond to the main glycine conformer **I**.

4.3. Separation of the Vibrational Bands of the Glycine Conformers. *C═O Stretching Vibrations*. The separation of the conformer bands in the matrix IR spectra starts with the analysis of the most intensive spectral features. The region of the C═O stretching vibrations of glycine-d_0 is presented in Figure 4. In this region of the spectrum, one very intensive band, as well the less intensive bands, are observed. The intensive bands at 1779, 1776, 1768, and 1769 cm^{-1} in the

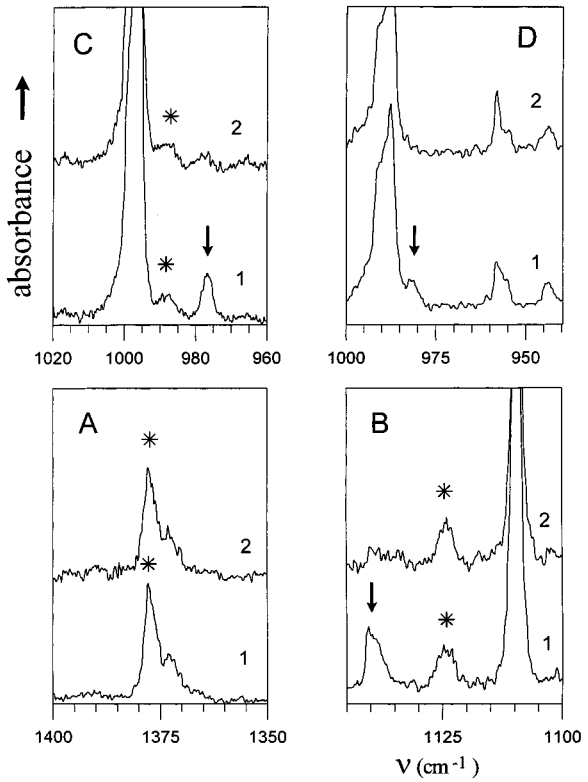

Figure 5. IR spectral regions of the glycine isotopomers: glycine-d_2 (A and B), glycine-d_3 (C), and glycine-d_5 (D). (1) IR spectrum recorded after matrix deposition at 13 K. (2) IR spectrum recorded after matrix annealing at 20 K for 30 min. Asterisks (*) mark the bands assigned to conformer **II**. Down arrows (↓) mark the bands assigned to conformer **III**.

spectra of the d_0, d_2, d_3, and d_5 isotopomers, respectively, are assigned to the C═O stretching vibrations of the main conformer **I**. The assignment of the less intensive bands is based on the results of the frequency calculations (Tables 5−8).

For all isotopomers, the high-frequency experimental band in the region of the C═O stretching vibration is assigned to the C═O vibration of conformer **II**, and the low-frequency band is assigned to the C═O vibration of conformer **III**. This assignment is confirmed by comparison of the spectra recorded before and after matrix annealing. The intensity of the bands of conformer **III** in the spectra of all glycine isotopomers must decrease significantly after sample heating due to the conformer **III** ⇒ conformer **I** interconversion. These bands are marked in Tables 5−8. Some relevant regions of the spectrum of glycine-d_0 are presented in Figures 4−6. As seen in Figure 4 and in Tables 5−8, the intensity of the bands assigned to the C═O stretching vibrations decreases significantly after matrix heating, which supports their proposed assignment.

In the case of the most intensive experimental bands, it was very important to prove that the origin of these bands is not due to site splitting. The region of the C═O stretching vibrations was studied in our preliminary work, where we used different matrix gases, and we demonstrated that the observed phenomenon is not caused by site splitting.[22] It is also important to mention that the site splitting is observed in the glycine spectra and some bands or, more often, band shoulders are definitely due to the matrix splitting. For example, the low-frequency shoulder at 1773 cm^{-1} on the band of the C═O stretching vibration of the conformer **I** (Table 5, Figure 4) is probably due to site splitting.

The comparison of the calculated and observed intensities of the C═O stretching vibrations of the three glycine conformers

TABLE 5: Observed and Calculated (at the DFT/B3LYP/aug-cc-pVDZ level) IR Frequencies (cm^{-1}) and Intensities of the Glycine-d_0

observed[a]			calculated						
			glycine **I**		glycine **II**		glycine **III**		
ν	A[b]	I_{obs}[c]	ν	I_{calcd}[d]	ν	I_{calcd}[d]	ν	I_{calcd}[d]	PED[e]
3560	0.253	3.111	3586	58.2			3584	65.8	OH str [100]
3543	0.041								
					3465	15.7			NH_8 str [57], NH_9 str [43]
3410	0.042	0.313	3429	5.3			3442	5.5	NH_8 str [50], NH_9 str [50]
					3384	0.4			NH_9 str [57], NH_8 str [42]
			3358	2.1			3366	2.5	NH_8 str [50], NH_9 str [50]
3200	0.029	0.522			3313	277.8			OH str [98]
			2962	6.3	2985	5.3	2968	4.9	CH_6 str [50], CH_7 str [50]
2958	0.023	0.826	2925	18.0	2938	12.1	2931	16.2	CH_6 str [50], CH_7 str [50]
2944	0.030								
1790	0.165	8.352			1813	355.4			C═O str [84]
1779	1.368		1787	292.5					C═O str [85]
1773*	0.217								
1767*	0.136						1779	296.3	C═O str [86]
1741	0.036	0.296							
1630	0.116	0.315	1641	18.1			1639	26.6	HNH bend [56], CNH bend [43]
1622	0.054	0.085			1630	31.6			HNH bend [60], CNH bend [39]
1429	0.097	0.341	1425	15.9	1432	5.3	1423	3.0	HCH bend [93]
1427	0.071								
1405	0.037	0.428							
1390	0.105	1.320			1396	373.1			COH bend [70], C−O str [10]
1383	0.107								
1373	0.050	0.092	1373	17.0					CCH bend [52], C−O str [12], COH bend [11], CC str t11]
			1359	0.0			1358	0.0	CCH bend [47], CCH bend [44]
1339*	0.079	0.430					1334	32.8	COH bend [33], C−O str [14]
					1331	5.3	1328	23.9	CCH bend [69]
					1302	10.2			CCH bend [70]
			1286	8.1					COH bend [45], CCH bend [28]
1210	0.050	0.092			1200	25.8			C−O str [46], CC str [20], GOH bend [18]
			1166	1.1			1170	3.1	CCH bend 162], CNH bend 132]
1147*	0.077	0.506					1161	238.2	C−O str [46], COH bend [42]
1136	0.082	2.009	1151	85.7	1146	2.1			CN str [37], C−O str [18]
1130	0.458								
1101	0.989	5.438	1113	217.7			1124	18.1	CN str [41], C−O str [36], COH bend [15]
1099	1.229								
					1059	15.9			CN str [80]
911	0.051	0.100			915	27.3			CCH bend [47], CNH_8 bend [17]
907	0.033	0.075	904	2.5			896	3.3	CNH bend 183]
883	0.485	1.749	898	103.8					CNH bend [22], CC str [18]
880	0.139				876	76.1			CC str [13], CCOH tor [13], C−O str [13]
867	0.109	0.378			852	81.2			CNH bend [54], GO str [17]
852*	0.079	0.213					866	120.0	CCOH tor [79]
809	0.134	0.425							
807	0.083								
801	1.233	3.948	808	89.1					CC str [41], C−O str [10]
798	1.056								
796	0.236								
786	0.126	0.305			804	41.3			CNH bend [31], CC str [23]
785	0.058								
777*	0.052	0.381					784	94.0	CC str [30], C−O str [24]
771*	0.063								
644*	0.036	0.660					675	99.8	CCOH tor [68], NCC═O tor [19]
619	0.346	2.642	642	90.8					CCOH tor [62], NCC−O tor [14]
617	0.771								
			624	5.1	633	5.1	586	46.6	CC═O bend [60], NCC bend [16]
					542	5.6			NCC═O tor [57], NCC−O tor [22]
500	0.195	1.431	508	28.1			511	20.3	CCOH tor [38], CCH bend [28]
498	0.180								
463	0.313	0.990	457	31.0	502	2.3	492	14.6	CC−O bend [66], CC str [16]
			253	10.3	305	17.9	257	2.1	NCC bend [49], O−C═O bend [47]
			202	43.0	246	14.6	232	45.0	CCNH tor 184], NCC−O tor [17]
			62	5.3	53	1.3	12	0.0	NCC−O tor [53], NCC═O tor [18]

[a] Ar matrix deposited at 13 K. Matrix ratio 1:1000. Asterisks (*) mark the bands which decreased after the matrix annealing at 20 K for 30 min. [b] A, experimental relative peak intensities. [c] I_{obs}, experimental relative integral intensities measured for the single bands or for the groups of the merged bands. [d] I_{calcd}, calculated intensities in km mol^{-1}. [e] PED contributions [%]. Only contributions ≥10% are listed. Abbreviations: str, stretching; bend, bending; tor, torsion.

also allows us to evaluate approximately the conformational composition of the gaseous glycine at the deposition temperature of ≈170 °C. Under this condition, about 70% of the compound exists as the main conformer **I**. The contributions of conformers

TABLE 6: Observed and Calculated (at the DFT/B3LYP/aug-cc-pVDZ level) IR Frequencies (cm^{-1}) and Intensities of the Glycine-d_2

observed[a]			calculated						
			glycine **I**		glycine **II**		glycine **III**		
ν	A[b]	I_{obs}[c]	ν	I_{calcd}[d]	ν	I_{calcd}[d]	ν	I_{calcd}[d]	PED[e]
3564	0.229	2.228	3586	58.3			3584	65.9	OH str [100]
					3464	15.9			NH_8 str [57], NH_9 str [43]
3410	0.032	0.205	3429	5.5			3442	5.7	NH_8 str [50], NH_9 str [50]
					3384	0.4			NH_9 str [57], NH_8 str [42]
			3358	2.3			3366	2.7	NH_8 str [50], NH_9 str [50]
3197	0.026	0.479			3313	277.4			OH str [98]
			2196	4.0	2216	3.7	2200	3.2	CD_6 str [50], CD_7 str [50]
			2130	12.2	2138	8.7	2134	11.9	CD_6 str [50], CD_7 str [50]
1794	0.214	0.948			1812	356.4			C═O str [84]
1776	0.865	6.979	1785	299.5					C═O str [86]
1770*	0.364						1778	299.4	C═O str [86]
1644	0.040	0.109	1639	18.2			1637	25.7	HNH bend [56], CCH bend [44]
					1629	30.6			HNH bend [60], CNH bend [40]
1378	0.187	1.028			1396	373.1			COH bend [71], C−O str [10]
1373	0.078								
1342*	0.036	0.161					1335	36.4	COH bend [41], C−O str [20]
1333	0.091	0.692	1332	33.4					COH bend [37], C−O str [21]
1330	0.117								
1291	0.030	0.288	1267	0.1	1232	8.2	1258	0.1	CNH bend [86]
1288	0.088								
1208	0.263	0.611	1209	29.9					CN str [31], COH bend [30]
1197	0.023	0.052			1201	25.6			C−O str [29], CNH_9 bend [18], CC str [16], COH bend [11]
1151*	0.082	0.204					1167	87.6	CN str [46], COH bend [18]
1141*	0.102	0.390					1157	185.3	C−O str [35], COH bend [26]
1125	0.073	0.296			1137	22.9			CN str [34], CCD_6 bend [21]
1109	0.877	2.079	1117	203.3					C−O str [35], CN str [32], COH bend [17]
1085	0.105	0.582							
1050	0.188	0.942	1045	63.4	1050	0.5	1049	6.7	DCD bend [81]
990	0.048	0.262	990	42.6					CCD bend [54], CN str [10]
981	0.086	0.498					985	25.4	CCD bend [54], CN str [17]
944	0.047	0.160	941	4.7			940	4.1	CCD bend [71], NCC═O tor [13]
					937	4.3			CN str [43], CCD bend [37]
					925	8.0			CCD bend [67], NCC−O tor [19]
831	0.401	2.033	849	110.5					CNH bend [60], CN str [19]
827	0.350								
825	0.115				863	96.4			CNH bend [38], CCOH tor [37]
818	0.052	0.182			852	88.1			CCOH tor [48], NCCO tor [13]
810*	0.074	0.319					826	136.8	CNH bend [63], CN str [15]
797	0.060	0.263	793	1.0	796	5.2	792	3.0	NCC═O tor [69]
788	0.655	1.543	784	42.0					CC str [47], CC−O bend [10]
783	0.065								
779	0.061	0.170			778	26.9			CCD bend [45], CNH bend [30]
769*	0.051	0.127					769	44.8	CC str [34], C−O str [32]
743	0.047	0.118							
732	0.038	0.320							
729	0.055								
629*	0.040	0.321					662	107.3	CCOH tor [83], NCC═O tor [11]
624	0.042		616	5.2	618	3.2			CC═O bend [60], NCC bend [17]
597	0.243	2.771	624	105.6					CCOH tor [82]
593	0.791								
585*	0.028	0.097					574	45.5	CC−O bend [63], NCC bend [19]
515	0.018	0.071			494	2.4	483	15.1	CC═O bend [53], CC str [25]
454	0.120	1.117	453	10.1			454	8.6	CCD bend [55], NCC−O tor [22]
449	0.063		448	30.2	472	4.7			CC−O bend [63], CC str [18]
445	0.053								NCC bend [16]
441	0.048								
			251	9.8	303	18.0	256	2.1	NCC bend [48], O═C−O bend [47]
			197	43.4	245	14.0	228	45.0	CCNH tor [88], NCC−O tor [12]
			57	4.6	48	0.9	8	0.0	NCC−O tor [52], CCD bend [26]

[a] Ar matrix deposited at 13 K. Matrix ratio 1:750. Asterisks (*) mark the bands which decreased after the matrix annealing at 20 K for 30 min. [b] A, experimental relative peak intensities. [c] I_{obs}, experimental relative integral intensities measured for the single bands or for the groups of the merged bands. [d] I_{calcd}, calculated intensities in km mol^{-1}. [e] PED contributions [%]. Only contributions ≥10% are listed. Abbreviations: str, stretching; bend, bending; tor, torsion.

II and **III** are approximately even and equal to 15%. This is in agreement with the results of the electron diffraction study of glycine,[2] where the main glycine conformer was determined to contribute ≈76% to the mixture.

O−H (O−D) Stretching Vibrations. In the high-frequency region of the spectra, the most intensive bands at 3560 (Table 5) and 3564 cm^{-1} (Table 6) are assigned to the OH stretching vibrations of glycine-d_0 and glycine-d_2, respectively. The bands at 2631 (Table 7) and 2630 cm^{-1} (Table 8) are assigned to the OD stretching vibrations of the glycine-d_3 and glycine-d_5. The

TABLE 7: Observed and Calculated (at the DFT/B3LYP/aug-cc-pVDZ level) IR Frequencies (cm^{-1}) and Intensities of the Glycine-d_3

observed[a]			calculated						
			glycine **I**		glycine **II**		glycine **III**		
ν	A[b]	I_{obs}[c]	ν	I_{calcd}[d]	ν	I_{calcd}[d]	ν	I_{calcd}[d]	PED[e]
			2962	6.0	2986	4.7	2968	4.6	CH_6 str [50], CH_7 str [50]
2948	0.035	0.352	2926	17.5	2938	13.1	2931	15.8	CH_6 str [50], CH_7 str [50]
2942	0.034								
2631	0.310	2.096	2609	38.0			2608	41.2	OD str [100]
					2556	9.8			ND_8 str [54], ND_9 str [46]
2551	0.030	0.134	2526	4.1			2536	4.1	ND_8 str [50], ND_9 str [50]
					2448	0.4			ND_9 str [53], ND_8 str [44]
2405	0.019	0.124	2429	2.7			2434	3.1	ND_8 str [50], ND_9 str [50]
2391	0.040	0.289			2411	148.5			OD str [97]
1788	0.333	10.702			1804	361.4			C═O str [87]
1768	1.720		1779	275.0					C═O str [88]
1764	0.165								
1756*	0.104						1770	282.7	C═O str [89]
1727	0.038	0.128							
1430	0.028								
1426	0.159	0.687	1425	14.8	1433	8.0	1423	3.3	HCH bend [97]
1424	0.102								
1377	0.160	0.490	1370	12.8					CCH bend [67], CC str [10]
1344*	0.055	0.095					1340	28.7	CCH bend [79]
1325	0.030	0.047			1318	29.0			CCH bend [81]
1283	0.113	0.505	1282	0.0	1284	24a.9	1289	0.2	C−O str [44], CC str [16], COD bend [16]
1273*	0.102	0.533					1271	185.9	C−O str [38], CC str [22]
1269	0.057								
1256	0.030	0.277			1255	6.3			CCH bend [77]
1253	0.029								
1248	0.029								
1220	0.596	5.331	1222	123.5	1211	40.7	1209	7.3	DND bend [61], CN str [15]
1217	0.759								
1215	1.251								
1200	0.066	0.217	1203	78.2					C−O str [25], CCH bend [22]
1081	0.061	0.376	1078	19.5			1072	20.8	CN str [66], CND bend [16]
1078	0.074								
1065	0.044	0.199	1066	1.8	1041	2.3	1062	2.0	CCH bend [30], CND bend [76]
					1014	14.7			CN str [70]
997	0.540	2.874	1002	95.7					COD bend [47], C−O str [31]
996	0.584								
987	0.036	0.199			994	27.4			COD bend [66], C−O str [14]
977*	0.061	0.234					993	82.2	COD bend [57], C−O str [24]
860	0.017	0.224			860	36.0			CC str [37], C−O str [31]
821	0.060	0.607	818	18.9					CC str [39], NCC bend [17],
818	0.058								COD bend [16]
803	0.025	0.076					800	23.8	CC str [35], C−O str [24]
793	0.031	0.202	781	3.4	776	4.0	776	4.8	CND bend [60]
785	0.054	0.302							
781	0.041								
686	0.711	2.997	692	87.4					CND bend [54], CC str [19],
684	0.893								COD bend [10]
663*	0.118	0.303					666	93.4	CND bend [60], CC str [15]
659	0.065	0.247			664	35.5			CND bend [63], NCC bend [12]
614	0.018	0.046			621	40.8			CCOD tor [96]
599	0.086	0.323			589	20.0			CC−O bend [32], NCC bend [17]
595	0.026						583	26.5	NCC═O tor [46], NCC−O tor [23]
575	0.049	0.688	573	20.4					CCH bend [34], NCC−O tor [25],
571	0.071								NCC═O tor [14], CCOD tor [11]
			569	0.9					CC═O bend [55], C−O str [11]
					535	6.0			NCC═O tor [49], NCC−O tor [19]
535*	0.032	0.237					529	39.2	CC−O bend [49], COD bend [16],
527*	0.021								CC═O bend [14]
501	0.010	0.040			493	2.6			CC═O bend [60], CC str [22]
481*	0.020	0.113					474	22.5	CC═O bend [53], CC str [15]
477*	0.009								
444	0.022	0.073							
437	0.471	1.369	431	35.9					CC−O bend [68], CC str [12]
419*	0.050	0.299					429	38.5	CCOD tor [82], NCC═O tor [11]
412	0.031								
			413	45.3					CCOD tor [89]
			236	10.7	280	15.1	238	2.8	NCC bend [51], O−C═O bend [42]
			159	21.2	195	7.7	177	24.3	CCND for [77], NCC−O for [24]
			54	5.2	47	1.4	8	0.0	NCC−O for [46], NCC═O for [22]

[a] Ar matrix deposited at 13 K. Matrix ratio 1:750. Asterisks (*) mark the bands which decreased after the matrix annealing at 20 K for 30 min. [b] A, experimental relative peak intensities. [c] I_{obs}, experimental relative integral intensities measured for the single bands or for the groups of the merged bands. [d] I_{calcd}, calculated intensities in km mol^{-1}. [e] PED contributions [%]. Only contributions ≥10% are listed. Abbreviations: str, stretching; bend, bending; tor, torsion.

TABLE 8: Observed and Calculated (at the DFT/B3LYP/aug-cc-pVDZ level) IR Frequencies (cm^{-1}) and Intensities of the Glycine-d_5

observed[a]			calculated						
			glycine **I**		glycine **II**		glycine **III**		
ν	A[b]	I_{obs}[c]	ν	I_{calcd}[d]	ν	I_{calcd}[d]	ν	I_{calcd}[d]	PED[e]
2630	0.188	1.189	2609	37.7			2608	41.2	OD str [100]
2626	0.120								
2575	0.012	0.086			2556	9.5			ND_8 str [54], ND_9 str [46]
2545	0.015	0.148	2526	3.8			2537	3.9	ND_8 str [50], ND_9 str [50]
					2449	0.5			ND_9 str [53], ND_8 str [44]
2411	0.015	0.068	2429	2.4			2435	2.7	ND_8 str [50], ND_9 str [50]
2399	0.021	0.284			2411	149.3			OD str [97]
2388	0.015								
			2195	4.2	2216	3.8	2200	3.2	CD_6 str [50], CD_7 str [50]
2155	0.012	0.098	2130	13.1	2138	8.1	2134	12.5	CD_6 str [50], CD_7 str [50]
1794	0.065	0.326							
1786	0.148	0.716			1803	363.2			C═O str [88]
1769	0.804	5.134	1777	281.4					C═O str [89]
1763*	0.094						1769	285.0	C═O str [90]
1719	0.024	0.058							
1308	0.046	0.181							
1298	0.133	1.528	1290	56.2					C−O str [25], CC str [22],
1295	0.216								CC═O bend [16], CN str [13]
1285	0.046	0.502			1286	269.8			C−O str [45], CC str [22],
1283	0.054								CC═O bend [14], COD bend [13]
1280	0.070								
1270*	0.059	0.198					1281	171.0	C−O str [29], CC str [25], CC═O bend[12], CN str [10]
1220*	0.025	0.142					1225	36.3	DND bend [54], CN str [15]
1208	0.825	1.636	1221	115.1					DND bend [53], CO str [14]
1195	0.042	0.113			1217	40.2			DND bend [77], CN str [18]
1120	0.119	0.482	1113	50.1					CN str [33], CCD bend [28]
1112*	0.017	0.069			1124	20.0	1121	36.1	CCD bend [28], CN str [22]
1102	0.021	0.128							
1099	0.020								
1050	0.055	0.576			1050	1.4	1045	2.0	DCD bend [60], CCD bend [26
1042	0.028		1045	0.0			1040	0.0	CND bend [56]
1021	0.028	0.260	1039	38.3					CCD bend [48], DCD bend [27]
					1006	3.9			CND bend t68]
991	0.137	1.244	1001	70.0					COD bend [50], C−O str [26]
988	0 194								
981*	0 025	0.094			994	26.8	992	74.2	COD bend [59], C−O str [21]
958	0.041	0.146	953	5.0			954	6.8	CCD bend [36], CN str [28]
955	0.023								
944	0.019	0.060	940	3.8	924	4.8	939	4.0	CCD bend [69], NCC═O tor [18]
					913	10.8			CN str [50], CCD bend [23]
810	0.028	0.061			807	25.9			CC str [31], C−O str [26]
767	0.084	0.274	764	19.2					CC str [27], CCD bend [24]
761	0.018	0.101					752	16.7	CC str [26], C−O str [22]
720	0.025	0.264	715	2.3	719	3.2	715	4.0	NCC═O tor [45], CND bend [40]
711	0.022								
708	0.026								
686	0.400	1.708	690	85.3					CND bend [50], CC str [23],
684	0.424								COD bend [12]
663*	0.062	0.139					666	92.4	CND bend [58], CC str [16]
658	0.041	0.201			658	38.2			CND bend [58J
599	0.047	0.130			619	42.7			CCOD tor [96]
593	0.015	0.117							
590	0.020								
573	0.011	0.034	566	1.0	577	15.6			CC−O bend [39], NCC bend [21]
528*	0.018	0.057					537	40.8	CCOD tor [41], NCC═O tor [35]
511	0.063	0.677	516	35.1			522	39.3	CCOD tor [33], NCC−O tor [21]
508	0.100								
					487	2.8	466	22.3	CC═O bend [55], CC str [17]
					463	4.4			NCC═O tor [51], CCD bend [21]
434	0.024	0.119							
428	0.257	0.816	423	34.8					CC−O bend [66], CC str [16]
			393	28.7			403	21.7	CCOD tor [68], CCD bend [20]
			234	10.3	279	15.1	236	2 7	NCC bend [50], O−C═O bend [42]
			153	21.5	192	7.1	172	24.3	CCND tor [81], NCC−O tor [19]
			51	4.7	43	1.0	5	0.0	NCC−O tor [47], NCC═O tor [17]

[a] Ar matrix deposited at 13 K. Matrix ratio 1:750. Asterisks (*) mark the bands which decreased after the matrix annealing at 20 K for 30 min. [b] A, experimental relative peak intensities. [c] I_{obs}, experimental relative integral intensities measured for the single bands or for the groups of the merged bands. [d] I_{calcd}, calculated intensities in km mol^{-1}. [e] PED contributions [%]. Only contributions ≥10% are listed. Abbreviations: str, stretching; bend, bending; tor, torsion.

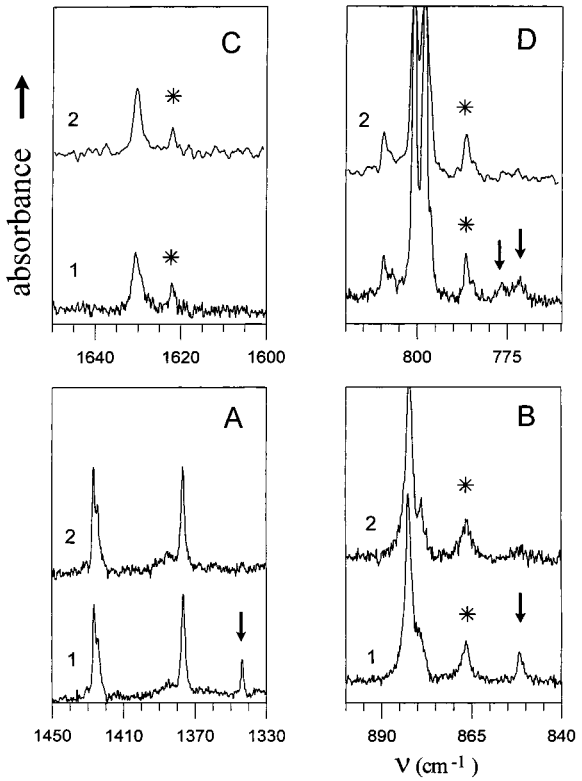

Figure 6. IR spectral regions of the glycine-d_0. OH bending/C−O stretching vibration region (A), CCOH torsion/NH_2 bending vibration region (B), NH_2 scissors vibration region (C), NH_2 bending vibration region (D). (1) IR spectrum recorded after matrix deposition at 13 K. (2) IR spectrum recorded after matrix annealing at 20 K for 30 min. Asterisks (*) mark the bands assigned to conformer **II**. Down arrows (↓) mark the bands assigned to conformer **III**.

calculations show that the OH(D) stretching vibrations of conformers **I** and **III** are very close and cannot be separated in the experimental spectra. On the other hand, the OH(D) stretching vibrations of conformer **II** is significantly downshifted due to formation of the intramolecular N···H−O H-bond. The frequency shift is 360 cm^{-1} for the OH stretch (Table 5) and 240 cm^{-1} for the OD stretch (Table 6). The calculations predict a considerable increase of the intensities of the OH(D) stretching vibrations of the conformer **II** due to H-bonding and this higher intensity allows us to identify the bands of these vibrations in the spectra of all glycine isotopomers.

For the OH stretching vibrations, as well as for the CH and NH stretches, the observed differences between the experimental unharmonic and calculated harmonic frequencies are larger than for other vibrations. This difference is due to the significant unharmonicity of the large amplitude X(C,N,O)−H stretching vibrations. The use of the uniform scaling factor of 0.96 for the DFT/B3LYP/aug-cc-pVDZ frequencies of X(C,N,O) stretches improves the agreement between the calculated and observed frequencies in all cases except the OH stretching vibrations of conformer **II**. The difference is more than 100 cm^{-1} after scaling (Tables 5 and 6). We believe this is caused by a significant unharmonicity of this vibration due to the strongest intramolecular N···H−O H-bond in conformer **II** among all the conformers studied. This interaction changes the potential energy surface near the equilibrium position of the hydroxy hydrogen. Analysis of the spectra of the deuterated glycines supports this conclusion. The difference between the observed and calculated frequencies of the OD stretching vibration, with a much smaller amplitude, is the same as those for other vibrations in this region. The relatively stronger unharmonicity of the OH stretching vibrations of the conformer **II** also results in a decrease of the isotope ratio for this vibration (ν_{OHstr}/ν_{ODstr})- from the value of 1.354 for conformers **I** and **III** to 1.338.

O−H (O−D) Bending and C−O Stretching Vibrations. The PED analysis of the vibrations in the region 1400−1100 cm^{-1} allowed us to identify in the spectra the bands which can be assigned to mixed OH bending/C−O stretching vibrations. Similar coupling has also been found in the spectra of the carboxylic acids.[33,34] The frequencies and PEDs of these vibrations are sufficiently different for the three glycine conformers to allow their assignment. The intensive experimental band at 1390 cm^{-1} in the spectrum of glycine-d_0 (Figure 5a) is assigned to the OH bending vibration of conformer **II**. This band is shifted toward higher frequencies, as compared to the corresponding bands of conformers **I** and **III**. The OH bending vibration of conformer **II** is the most intensive vibration. This band may be easily recognized in the IR spectra and may serve as one of the main spectral manifestations of the conformer-**II**-like conformations of aminoacids. The other band at 1200 cm^{-1} is also assigned to the vibration of conformer **II**. This vibration has a very complex mode with contributions from the C−O stretching, the CC stretching and the OH bending modes. Two bands in this region with contributions from the OH bending and the C−O stretching modes are assigned to the vibrations of conformer **III**. The intensities of these bands decrease in the spectra after matrix annealing and this fact supports the assignment of these bands. In the spectra of glycine-d_3 and glycine-d_5 (Tables 7 and 8), the vibrations with the contribution from the OD bending mode are observed in the range 1000−800 cm^{-1}. This low-frequency shift of the OD bending vibration allows us to identify the vibrations with large contributions from the C−O stretching mode in the spectra of the deuterated glycine. The assignment and PEDs of these bands are presented in Tables 7 and 8.

N−H (N−D) Stretching and Bending Vibrations. The NH stretching vibrations, both symmetrical and asymmetrical, have very low intensity and in the experimental spectra only the weak band of the NH asymmetrical stretching vibration at 3410 cm^{-1} was detected (Table 5). At the same time, the bands attributed to the NH bending vibrations are more intensive. The NH scissors vibrations are observed in the region 1650−1600 cm^{-1} (glycine-d_0 and glycine-d_2) or in the region 1250−1200 cm^{-1} (glycine-d_3 and glycine-d_5). The band of the NH scissors vibration of conformer **II** at 1622 cm^{-1} and the corresponding band of conformer **I** at 1630 cm^{-1} are identified in the spectrum of glycine-d_0 (Table 5, Figure 6). The small difference (8 cm^{-1}) between the frequencies of the NH bending vibrations of conformers **I** and **II**, as well as the relatively small difference between the NH stretching vibrations of these conformers (less than 40 cm^{-1}, Table 5) demonstrate the weakness of the N−H···O H-bonding interaction in conformers **I** and **III**. The corresponding values obtained for the OH bending and stretching vibrations are ≈100 and 360 cm^{-1}. This is the spectroscopic evidence of the significant difference between the N−H···O and N···H−O intramolecular interactions in the glycine conformers. It indicates that the NH_2 group is a good proton acceptor but a less effective proton donor.

The data presented in Tables 5−8 and in Figures 7 and 8 allows us to identify some other vibrations of the minor glycine conformers in the region below 1000 cm^{-1}. The OH torsional vibrations should be mentioned here in the first hand. Three bands in the spectra at 619, 852 and 644 cm^{-1} are attributed to the OH torsional vibrations of conformers **I**, **II**, and **III**,

TABLE 9: Experimental (Ar matrix) and Calculated (DFT/B3LYP/aug-cc-pVDZ) IR Spectral Characteristics of the Glycine Minor Conformer II[a]

ν_{obs}	ν_{calc}	assignment	ν_{obs}	ν_{calc}	assignment
	Glycine-d_0			Glycine-d_2	
3200	3313	OH str	3197	3313	OH str
1790	1813	C═O str	1794	1812	C═O str
1622	1630	HNH bend	1378	1396	OH bend
1390	1396	OH bend	1197	1201	C−O str
1210	1210	C−O str	1125	1137	CN str
911	915	CH bend	818	852	COOH tor
867	852	CCOH tor	779	778	CD bend
786	604	CNH bend			
	Glycine-d_3			Glycine-d_5	
2391	2411	OD str	2399	2411	OD str
1788	1804	C═O str	1786	1803	C═O str
1325	1318	CH bend	1285	1286	C−O str
1283	1284	C−O str	1195	1217	ND bend
1256	1255	CH bend	810	807	CC str
987	994	OD bend	658	658	ND bend
860	869	CC str	599	619	CCOD tor
659	664	ND bend	573	577	C−O bend
614	621	CCOD tor			
S99	589	C−O bend			

[a] Abbreviations: str, stretching; bend, bending; tor, torsion.

TABLE 10: Experimental (Ar matrix) and Calculated (DFT/B3LYP/aug-cc-pVDZ) IR Spectral Characteristics of the Glycine Minor Conformer III[a]

ν_{obs}	ν_{calc}	assignment	ν_{obs}	ν_{calc}	assignment
	Glycine-d_0			Glycine-d_2	
1767	1779	C═O str	1770	1778	C═O str
1339	1334	OH bend, C−O str	1342	1335	OH bend, C−O str
1147	1161	C−O str, OH bend	1151	1167	CN str
852	866	NH bend	1141	1151	C−O str, OH bend
777	784	CC str	810	826	NH bend
644	675	CCOH tor	769	769	CC str
			629	662	CCOH tor
			585	574	C−O bend
	Glycine-d_3			Glycine-d_5	
1756	1770	C═O str	1763	1769	C═O str
1344	1340	CH bend	1270	1281	C−O str
1273	1271	C−O str	1220	1225	ND bend
1081	1072	CN str	1112	1121	CD bend
977	993	OD bend	981	992	OD bend
803	800	CC str	761	752	CC str
663	666	ND bend	663	666	ND bend
595	583	NCC═O tor			
528	537	CCOD tor			
535	529	C−O bend			
481	474	C═O bend			
419	429	CCOD tor			

[a] Abbreviations: str, stretching; bend, bending; tor, torsion.

respectively. The observed frequency of the OH torsional vibration of conformer **II**, like ones of the OH stretching and bending vibrations of this conformer, are significantly different from the corresponding vibrations of conformers **I** and **III** due to the intramolecular H-bonding.

Finally, we collected all frequencies attributed to the vibrations of the minor conformers **II** and **III** in Tables 9 and 10. For these conformers we also evaluated the mean divergences between the observed and calculated (at the DFT/B3LYP/aug-cc-pVDZ level) frequencies. These divergences are very close to the values obtained for conformer **I** (Table 4). For example, the mean divergences calculated for conformers **II** and **III** of the glycine-d_0 are 7.6 and 11.8 cm^{-1}, respectively. This provides additional support to our assignment of the experimental bands in the matrix IR spectra.

5. Conclusions

In this study we have applied matrix isolation IR spectroscopy and correlated ab initio calculations to investigate the conformational behavior of the simplest aminoacid−glycine. We obtained an experimental confirmation of the presence of a new glycine conformer with the NH_2···O-C bifurcated H-bond in the argon matrices. The IR spectral characteristics of the three rotational conformers of the glycine were determined for the first time. The analysis and assignment of the experimental matrix IR spectra made in this work are based on three sources: the results of theoretical simulations of the vibrational frequencies and intensities of the conformers, the spectral manifestations of the conformational interconversion conformer **III** ⇒ conformer **I** which occurs upon matrix annealing, and the spectra obtained for glycine deuterated derivatives.

A very good agreement between experimental and calculated (at the DFT/B3LYP/aug-cc-pVDZ and MP2/aug-cc-pVDZ levels of theory) spectra was found. This suggests that the DFT/B3LYP/aug-cc-pVDZ level of theory may be successfully applied to reproduce the structure, relative stabilities and IR spectral characteristics of nonionized aminoacid and oligopeptide conformers and can be used in assignment of their IR spectra.

We also demonstrated that the IR spectral differences between the three glycine conformers are caused by different intramolecular H-bonding interactions in these conformers. Analysis of the frequency shifts of the OH and NH stretching and bending vibrations affected by the H-bonding indicates that the N···H−O H-bond in the conformer **II** is much stronger than the NH···O H-bonds in conformers **I** and **III**.

Acknowledgment. This work was supported a COBASE grant allowing the visit of Dr. S. Stepanian to the University of Arizona. The authors also acknowledge partial support from J.N.I.C.T., the PRAXIS XXI (Grant 2/2.1/QUI/412/94), and FEDER.

References and Notes

(1) l. Almlöf, J.; Kuick, A.; Thomas, J. O. *J. Chem. Phys.* **1973**, *59*, 3901.
(2) Iijima, K.; Tanaka, K.; Onuma, S. *J. Mol. Struct.* **1991**, *246*, 257.
(3) (a) Snyder, L. E.; Hollis, J. M.; Suenram, R. D.; Lovas, F. J.; Brown, L. W.; Buhl, D. *Astrophys. J.* **1983**, *268*, 123. (b) Berulis, I. I.; Winnewisser, G.; Krasnov, V. V.; Sorochenko, R. L. *Sov. Astron. Lett.* **1985**, *11*, 251.
(4) Brown, R. D.; Godfrey, P. D.; Storey, J. W. V.; Bassez, M. P. *J. Chem. Soc., Chem. Commun.* **1978**, 547.
(5) Suenram, R. D.; Lovas, F. J. *J. Mol. Spectrosc.* **1978**, *72*, 372.
(6) (a) Vishveshwara, S.; Pople, J. A. *J. Am. Chem. Soc.* **1977**, *99*, 2422. (b) Sellers, H. L.; Schäfer, L. *J. Am. Chem. Soc.* **1978**, *100*, 7728.
(7) (a) Suenram, R. D.; Lovas, F. J. *J. Am. Chem. Soc.* **1980**, *102*, 7180. (b) Schäfer, L.; Sellers, H. L.; Lowas, F. J.; Suernam, R. D. *J. Am. Chem. Soc.* **1980**, *102*, 6566.
(8) Godfrey, P. D.; Brown, R. D. *J. Am. Chem. Soc.* **1995**, *117*, 2019.
(9) Lovas, F. J.; Kawashima, Y.; Grabow, J.-U.; Suenram, R. D.; Freser, G. T.; Hirota, E. *Astrophys. J.* **1995**, *455*, 201.
(10) Yu, D.; Rauk, A.; Armstrong, D. A. *J. Am. Chem. Soc.* **1995**, *117*, 1789.
(11) Barone, V.; Adamo, C.; Lelj, F. *J. Chem. Phys.* **1995**, *102*, 364.
(12) Császár, A. *J. Mol. Struct.* **1995**, *346*, 141.
(13) Hoyau, S.; Ohanessian, G. *J. Am. Chem. Soc.* **1997**, *119*, 2016.
(14) Lelj, F.; Adamo, C.; Barone, V. *Chem. Phys. Lett.* **1994**, *230*, 189.
(15) Hu, C. H.; Shen, M.; Schaefer, H. F. *J. Am. Chem. Soc.* **1993**, *115*, 2923.
(16) Császár, A. *J. Am. Chem. Soc.* **1992**, *114*, 9568.
(17) Frey, R. F.; Coffin, J.; Newton, S. Q.; Ramek, M.; Cheng, V. K. W.; Momany, F. A.; Schäfer, L. *J. Am. Chem. Soc.* **1992**, *114*, 5369.
(18) Yu, D.; Armstrong, D. A.; Rauk, A. *Can. J. Chem.* **1992**, *70*, 1762.
(19) l9. Jensen, J. H.; Gordon, M. S. *J. Am. Chem. Soc.* **1991**, *113*, 7917.
(20) Ramek, M.; Cheng, V. K. W.; Frey, R. F.; Newton, S. Q.; Schäfer, L. *J. Mol. Struct. (THEOCHEM)* **1991**, *235*, 1.
(21) The matrix-isolation IR spectroscopy was successfully applied to study the molecular structure of the nucleic acid bases having very low

vapor pressure over the solid state. For example, see: Sheina, G. G.; Stepanian S. G.; Radchenko, E. D.; Blagoi, Yu, P. *J. Mol. Struct.* **1987**, *158*, 275 and works cited therein.

(22) Reva, I. D.; Plokhotnichenko, A. M.; Stepanian, S. G.; Ivanov, A. Yu.; Radchenko, E. D.; Sheina, G. G.; Blagoi, Yu, P. *Chem. Phys. Lett.* **1995**, *232*, 141. Erratum. *Chem. Phys. Lett.* **1995**, *235*, 617.

(23) (a) Grenie, Y.; Lassegues, J. C.; Garrigou-Lagrange, C. *J. Chem. Phys.* **1970**, *53*, 2980. (b) Grenie, Y.; Garrigou-Lagrange, C. *J. Mol. Spectrosc.* 1972, *41*, 240.

(24) Radchenko, E. D., Sheina, G. G.; Smorygo N. A.; Blagoi Yu, P. *J. Mol. Struct.* **1984**, *116*, 387.

(25) (a) Binkley, J. S.; Pople, J. A. *Int. J. Quantum Chem.* **1975**, *9*, 229. (b) Pople, J. A.; Binkley, J. S.; Seeger, R. *Int. J. Quantum Chem., Quantum. Chem. Symp.* **1976**, *10*, 1.

(26) Becke, A. D. *Phys. Rev. B* **1988**, *38*, 3098.

(27) Lee, C.; Yang, W.; Parr, R. G. *Phys. Rev. B* **1988**, *37*, 785.

(28) Vosko, S. H.; Wilk, L.; Nusair, M. *Can. J. Phys.* **1980**, *58*, 1200.

(29) Woon, D. E.; Dunning, T. H. *J. Chem. Phys.* **1993**, *98*, 1358.

(30) Kendall, R. A.; Dunning, T. H.; Harrison, R. J. *J. Chem. Phys.* **1992**, *96*, 6796.

(31) Dunning, T. H. *J. Chem. Phys.* **1989**, *90*, 1007.

(32) Frisch, M. J.; Trucks, G. W.; Schlegel, H. B.; Gill, P. M. W.; Johnson, B. G.; Robb, M. A.; Cheeseman, J. R.; Keith, T.; Petersson, G. A.; Montgomery, J. A.; Raghavachari, K.; Al-Laham, M. A.; Zakrzewski, V. G.; Ortiz, J. V.; Foresman, J. B.; Cioslowski, J.; Stefanov, B. B.; Nanayakkara, A.; Challacombe, M.; Peng, C. Y.; Ayala, P. Y.; Chen, W.; Wong, M. W.; Andres, J. L.; Replogle, E. S.; Gomperts, R.; Martin, R. L.; Fox, D. J.; Binkley, J. S.; Defrees, D. J.; Baker, J.; Stewart, J. P.; Head-Gordon, M.; Gonzalez, C.; Pople, J. A. *Gaussian 94, Revision E.2*; Gaussian, Inc.; Pittsburgh, PA, 1994.

(33) Reva, I. D.; Plokhotnichenko, A. M.; Radchenko E. D.; Sheina, G. G.; Blagoi, Yu, P. *Spectrochim. Acta* **1994**, *50A*, 1107.

(34) Stepanian S. G.; Reva, I. D.; Radchenko, E. D.; Sheina, G. G. *Vib. Spectr.* **1996**, *11*, 123.